

Lectures by Our Lab.



SIELA 2014

Technical
University
of Sofia

XVIIIth International Symposium on
Electrical Apparatus and Technologies
29 – 31 May, 2014
Bourgas, Bulgaria

Harmonic Balance for Magnetization Characteristics Exhibiting Hysteretic Property

Hideaki Nemori and Yoshifuru Saito

Graduate School of Electrical and Electronics Engineering
Hosei University
Tokyo 184-8584, Japan
Email address: hideaki.nemori.4p@stu.hosei.ac.jp

Iliana Marinova

Department of Electrical Apparatus
Technical University of Sofia
Sofia, Bulgaria
E-mail address: iliana@tu-sofia.bg

Abstract—The present paper proposes one of the Domain based hysteretic constitutive equations utilizing the orthogonal property of the sinusoidal and cosinusoidal periodic function. At first, we assume a magnetic domain based constitutive equation. Second, to determine the coefficients of the assumed constitutive equation, we applied orthogonal properties of the sinusoidal and cosinusoidal functions. To check the validity of our constitutive equation, we carried out numerical as well as experimental verifications.

Keywords—harmonic balance; hysteretic property; orthogonal property

I. INTRODUCTION

As is well known, a representative ferromagnetic material is the iron which is commonly used as the frame structural materials of many artificial products. Ferromagnetic materials exhibit a lot of complex physical properties, such as magnetization, magnetostriction and magneto-thermodynamic properties. Ferromagnetic materials are composed of magnetic domains and exhibit nonlinear hysteretic magnetization characteristics. Particularly, their nonlinear magnetization characteristics are function of externally impressed stresses. This is because some external physical energy is added to their domain structures so that their structures are essentially stimulated to change. This means that parameters which characterize the magnetization characteristics of ferromagnetic materials may be considered as one of the possible soundness figures to represent their physical situation, e.g. under stressed or not.

We introduce a magnetic domain based constitutive equation to model the magnetization properties of ferromagnetic materials. And also, we describe this domain based model in conjunction with harmonic balance method. According to our formulation, a harmonic balance representation of the domain based model could be derived by means of the orthogonal property between the odd and even functions. Numerical as well as experimental verification of our method has been carried out. Further, we have revealed the differences of its parameters under stressed or not.

II. DOMAIN BASED MODEL

A. Domain Based Model and Its Parameters

Previously, we have proposed two types of constitution models for representing the ferromagnetic properties [1,2]. This paper employs the later proposed domain based model [2], and this domain based model is represented in terms of the magnetic field $H[A/m]$ and flux density $B[T]$. The domain based magnetization model is given by

$$H = \frac{1}{\mu} B + \frac{1}{s} \frac{dB}{dt} - \frac{\mu_r}{s} \frac{dH}{dt}, \quad (1)$$

where μ , μ_r and s are the permeability measured in the ideal magnetization curve, reversible permeability measured along with the ideal magnetization curve, and hysteresis coefficient, respectively.

B. Harmonic Balance Modeling

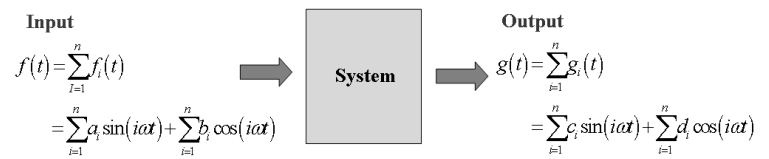


Fig. 1. Simple input and output system

Let us consider an input and output system shown in Fig.1. When the input and output of this system are respectively given by

$$f(t) = \sum_{i=0}^n a_i \sin(i\omega t) + \sum_{i=0}^n b_i \cos(i\omega t), \quad (2)$$

$$g(t) = \sum_{i=0}^n c_i \sin(i\omega t) + \sum_{i=0}^n d_i \cos(i\omega t), \quad (3)$$

we represent this system by a following constitutive equation

$$f(t) = \frac{1}{\mu} g(t) + \frac{1}{s} \frac{dg(t)}{dt} - \frac{\mu_r}{s} \frac{df(t)}{dt}. \quad (4)$$

An alternative form of (4) is

$$f(t) = \alpha g(t) + \beta \frac{dg(t)}{dt} - \gamma \frac{df(t)}{dt} \quad (5)$$

To determine the parameter α , β , γ , in (3), multiply the output function $g(t)$ to both sides of (3) and integrate from 0 to T yields.

$$\begin{aligned} & \int_0^T g(t) f(t) dt \\ &= \alpha \int_0^T g(t) g(t) dt + \beta \int_0^T g(t) \frac{dg(t)}{dt} dt - \gamma \int_0^T g(t) \frac{df(t)}{dt} dt \end{aligned} \quad (6)$$

Similarly multiply the time derivative of output function $dg(t)/dt$ to both sides of (3) and integrate from 0 to T yields

$$\begin{aligned} & \int_0^T \frac{dg(t)}{dt} f(t) dt \\ &= \alpha \int_0^T \frac{dg(t)}{dt} g(t) dt + \beta \int_0^T \frac{dg(t)}{dt} \frac{dg(t)}{dt} dt - \gamma \int_0^T \frac{dg(t)}{dt} \frac{df(t)}{dt} dt \end{aligned} \quad (7)$$

Further, multiply the input function $f(t)$ to both sides of Equation.(3) and integrate from 0 to T yields

$$\begin{aligned} & \int_0^T f(t) f(t) dt \\ &= \alpha \int_0^T f(t) g(t) dt + \beta \int_0^T f(t) \frac{dg(t)}{dt} dt - \gamma \int_0^T f(t) \frac{df(t)}{dt} dt \end{aligned} \quad (8)$$

Substituting the input (2) and output (3) functions into the equations (6), (7) and (8), it is possible to set up a system of equations for i -th harmonics as

$$\begin{bmatrix} a_i c_i + b_i d_i \\ b_i c_i - a_i d_i \\ a_i^2 + b_i^2 \end{bmatrix} = \begin{bmatrix} c_i^2 + d_i^2 & 0 & -\omega(a_i d_i - b_i c_i) \\ 0 & \omega(c_i^2 + d_i^2) & -\omega(a_i c_i + b_i d_i) \\ a_i c_i + b_i d_i & -\omega(a_i d_i - b_i c_i) & 0 \end{bmatrix} \cdot \begin{bmatrix} \alpha_i \\ \beta_i \\ \gamma_i \end{bmatrix}. \quad (9)$$

Input and output relation for i -th harmonics is given by

$$f_i(t) = \alpha_i g_i(t) + \beta_i \frac{dg_i(t)}{dt} - \gamma_i \frac{df_i(t)}{dt}. \quad (10)$$

Let us introduce a phaser notation, i.e., a symbol $\hat{\cdot}$ refers to complex quantities, then (10) could be reduced into

$$(1 + j\omega\gamma_i) \hat{f} = (\alpha_i + j\omega\beta_i) \hat{g}, \quad (11)$$

where

$$j = \sqrt{-1}. \quad (12)$$

Thus, the output is the real part of

$$\begin{aligned} \hat{g}_i(t) &= \frac{(1 + j\omega\gamma_i)}{(\alpha_i + j\omega\beta_i)} \hat{f}_i(t) \\ &= \sqrt{\frac{1 + (\omega\gamma_i)^2}{\alpha_i^2 + (\omega\beta_i)^2}} \sqrt{f_{i,r}^2 + f_{i,lm}^2} \\ &\quad \mathcal{E}^{j \tan^{-1} \frac{f_{i,lm}}{f_{i,r}} + j \tan^{-1} \omega\gamma_i - j \tan^{-1} \frac{\omega\beta_i}{\alpha_i}}, \end{aligned} \quad (13)$$

i.e.,

$$\begin{aligned} \hat{g}_i(t) &= \sqrt{\frac{1 + (\omega\gamma_i)^2}{\alpha_i^2 + (\omega\beta_i)^2}} \sqrt{f_{i,r}^2 + f_{i,lm}^2} \\ &\quad \cos\left(i\omega t - \tan^{-1} \frac{f_{i,lm}}{f_{i,r}} + \tan^{-1} \omega\gamma_i - \tan^{-1} \frac{\omega\beta_i}{\alpha_i}\right), \end{aligned} \quad (14)$$

Entire sum of the output (14) for i -th harmonics gives the output g of (3).

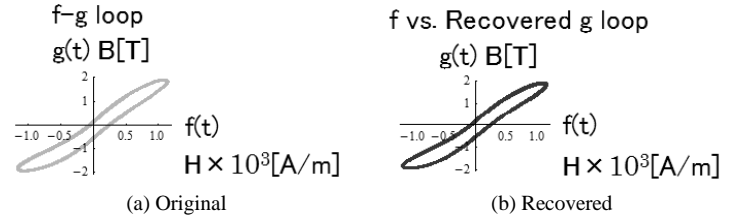


Fig. 2. Validity check of the model (4) or (5).

Figure 2 shows one of the examples of the recoverability of our domain based harmonic balance solution. According to the result shown in Fig.(1), it is obvious that the nonlinear magnetization characteristics exhibiting the hysteretic properties of ferromagnetic fields could be solved by means of phaser transform method.

C. Experiment

Figure 3 shows an experimental device and Table 1 lists its various constants. The tested specimens are the silicon steels with the 0.35mm thickness, 30mm width and 100mm length. The tested specimen was put on the upper two head surfaces of U shape ferrite core wound the 300 turns exciting coil. The specimen in Fig.1 is excited by flowing a 0.45A sinusoidal alternating current through this exciting coil.

Figure 4 shows a comparison between the experimented and recovered hysteresis loops.

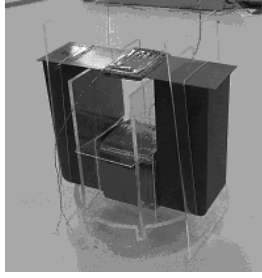
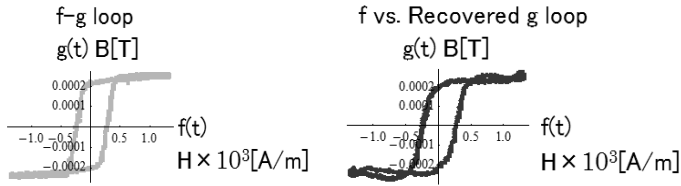


Fig. 3. Specimen and U shape ferrite core

TABLE I. SPECIFICATION OF THE MESUREMENT DEVICES

Specimen	U shape ferrite core
Material: silicon steels	Material: ferrite
Length: 100cm	Number of coil turns: 300 turns
Width: 30mm	Diameter of conductor: 0.6mm
Thickness: 0.35mm	
Number of coil turns: 300 turns	
Diameter of conductor: 0.2mm	



(a) Experimented

(b) Recovered by (14)

Fig. 4. Comparison between the experimental hysteresis loop and recovered hysteresis loop

Recovered hysteresis loop by (14) is well corresponding to experimental one. This means that the hysteretic nonlinear magnetization problems in ferromagnetic fields could be solved by means of the harmonic balance methodology.

D. Stress Visualization

Figure 5 shows an experimental scheme illustration to visualize the applied stress. A U shape ferrite core wound the exciting coil just same as shown in Fig.3. The specimen which wound the search coil is put on the upper two head surfaces of U shape ferrite core.

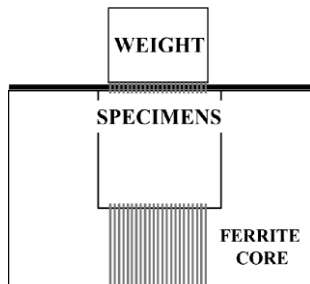


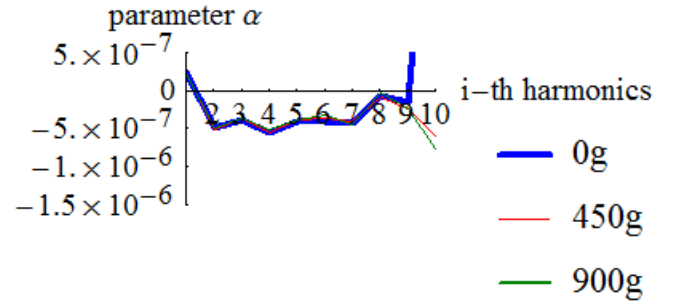
Fig. 5. The applied stress visualize scheme.

The stresses were applied to the specimen by putting on the wood weights to the specimen as shown in Figure 5. The used weights are 450 and 900 gram.

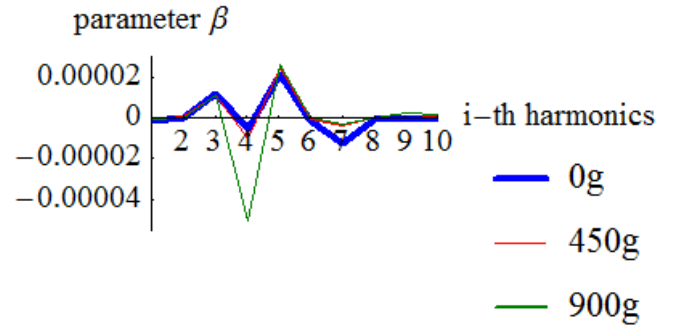
Figure 6 shows the parameters $\alpha_i, \beta_i, \gamma_i$ in (10) to each of the harmonics. According to the variation of β_i shown in Fig. 6(b), it is found that the parameter β_i is highly sensitive to the applied stress.

The parameter β_i corresponds to the 1st time derivative term as (5) so that this represents the hysteretic property of the ferromagnetic materials.

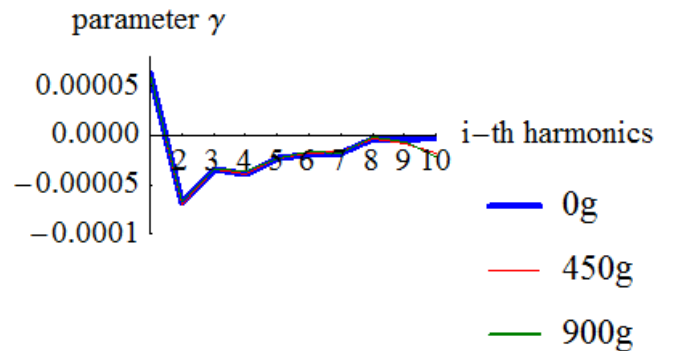
Thus, the external stress gives a large effect to the magnetic hysteresis, i.e., iron loss may be greatly increased by the externally applied stress. In the other words, the iron losses in the electrical machines distribute depending on the stress distribution and take the large in value at highly stressed positions.



(a) Parameter α



(b) Parameter β



(c) Parameter γ

Fig. 6. The relationships between the parameters $\alpha_i, \beta_i, \gamma_i$ in (10) and the order of harmonics when applied the different external stress.

III. CONCLUSIONS

The hysteretic nonlinear problems in ferromagnetic fields could be solved by means of the harmonic balance approach.

The parameters μ , μ_r and s in the domain based model could be determined in each of the harmonics by the Fourier approach.

According to our approach, it has been revealed that the parameter related to the time derivative term of the domain based model is highly sensitive to the applied stress. Namely, the iron losses in the electrical machines distribute depending

on the stress distribution and take the large in value at the highly stressed positions.

IV. REFERENCES

- [1] Y. Saito, Three dimensional analysis of magnetodynamic fields in electromagnetic devices taking into account the dynamic hysteresis loops, IEEE Transaction on Magnetics Vol.MAG-18 No.2 March 1982, pp.546-551.
- [2] S. Hayano, M.Namiki and Y.Saito, A magnetization model for computational magnetodynamics, Journal of Applied Physics Vo. 69, No.8, April 1991, pp.4614-4616.

Backside Defect Searching by Means of the Low Frequency ∞ Coil Excitation

Shunichi Hamanaka, Yoshifuru Saito
Graduate School of Electrical and Electronics Engineering
Hosei University,
Tokyo, Japan,
and
Iliana Marinova
Technical University of Sofia 1756,
Bulgaria

Manabu Ohuch, Hideo Mogi
and
Yoshiro Oikawa
Denshijiki Industry Co, Ltd
Tokyo, Japan,

Abstract— This paper describes the backside defect searching by means of the low frequency ∞ coil excitation. The low frequency ∞ coil excitation confronts to a noise processing problem in the practical tests. To overcome this difficulty, this paper employs two methodologies. One is an averaged sum and the other is the Fourier transform signal processing methods to reduce the higher frequency components compared to the excitation one. Thus, we have succeeded in enhancing the S/N ratio and detecting the signals caused by the backside defects of the targets. As a result, we have elucidated that the backside defect searching is possible by employing the low frequency excitation to our ∞ coil. Experimental as well as numerical verification along with intensive three-dimensional finite element method are carried out to confirm our results.

Keywords—Backside defect searching, Eddy current, Nondestructive testing, ∞ coil

V. INTRODUCTION

Modern engineering products such as air-plane, automobile, smart building, high speed train and so on are essentially composed of metallic materials for forming the shape of product, suspending the mechanical stress and constructing the structural frames.

In particular, the mass transportation vehicles, e.g. large air plane, high-speed train, express highway bus, carrying a large number of people are required the ultimate high safety as well as reliability.

To keep the high safety and reliability, nondestructive testing to the metallic materials is one of the most important key maintenance technologies because most of the structure materials are composed of the metallic materials.

Various nondestructive testing methods, such as eddy current testing (ECT), electric potential method, ultrasonic imaging and x-ray tomography are currently used to the modern airplane, high-speed -train and express high bus maintenance. Among these methods, ECT needs not complex electronic circuits and direct contact to the targets. And also,

most of the targets whose major frame parts are composed of conductive metallic materials can be selectively inspected by ECT [1-3].

Operation principle of ECT is fundamentally based on the magnetic field distribution change detection due to the defect in the targets. To realize this principle, we have two methodologies. One detects the defect in the target as a change of input impedance of the exciting coil. This is because the magnetic field distribution is changed by the detour eddy currents flowing around the defect in the target which corresponds to the secondary circuit of a single phase transformer [2-3]. The other type ETC sensor equips a sensing coil to detect the magnetic field change caused by the detour eddy currents flowing around the defect. The former and latter are called the impedance sensing and sensing coil types, respectively.

The sensing coil type is further classified into two variations. Most popular sensing coil type employs a differential coil, and also the other type sets the sensing coil surface perpendicularly to those of the exciting coil. As is well known the differential coil detects the uniformity of the magnetic field distribution. Similarly the perpendicularly installed sensing coil surface to those of exciting coil detects only the magnetic fields caused by the detour eddy currents due to the defect in the target.

Our developed ∞ coil one of the latter types, i.e., detects only the magnetic fields caused by the detour eddy currents due to the defect in the target. A key idea of our ∞ coil is that the sensing coil wound around a ferrite bar is installed at the lowest magnetic field intensity region between the north and south poles of exciting coils [1].

In the present paper, to search for the backside defect of a target, we have employed a low frequency excited ∞ coil. As a result, it is revealed that the ∞ coil has versatile capability, i.e., low frequency excitation of the ∞ coil makes it possible to detect the backside defects along with the signal processing methodologies.

VI. SIGNAL PROCESSING METHODS

A. Averaged Sum Method

In any signal measurement devices, it is essential to confront to the mixing of noise problems. Particularly, the low frequency excitation of ∞ coil measures a serious noise signal quantity compared with those of the desired one.

One of the common natures of any noise never repeat the same magnitude in value at the same periodic signal points. This means that an average of the same periodic signals reduces the noise signals. This signal processing methodology is the averaged sum approach, which is carried out to a M -th times measured signal $x(k)$ by

$$x(k) = \frac{1}{M} \sum_{i=1}^M x^i(k) = \frac{1}{M} \sum_{i=1}^M s^i(k) + \frac{1}{M} \sum_{i=1}^M n^i(k), \quad (1)$$

where s and n are the correct noise components, respectively.

B. Fourier Transform Method

The other methodology to remove the noise components from the measured signal is the Fourier transform method. Even though Fourier approach requires some mathematical operation or electronic circuits, it is one of the base technologies to synthesis the low-, high- and band pass filters.

To our ECT signal processing, we utilize the Fourier transform approach to pick up a particular frequency component from the measure signals, where the particular frequency is the same as those of the exciting frequency.

VII. EXPERIMENT

A theoretical background of the low exciting ECT is the skin effects, i.e., low frequency magnetic fields induce the eddy currents in the deep location of the metallic materials. Namely, the low frequency excitation of ECT makes it possible to detect the defects located in the deep or backside of the target metallic materials.

In our experiments, we have employed the two copper plates, one is the normal copper plane having 2mm thickness, 10cm length, 2mm width, and the other is the target having a 1mm defect at the backside.

Consideration of the skin depth to these targets has led to employ the 2kHz excitation frequency.

A. Averaged Sum Processing

Figure 1 shows a schematic diagram and Table 1 lists the various constants for the 3D finite element computations. Figure 2 shows one of the computed results, i.e., a large amplitude 5.1mV sensor signal has been obtained without any noise effects where the sensor is on the backside defect and is not on any defect.

Thus, theoretically it is possible to detect the backside defect by the low frequency excitation of the ∞ coil.

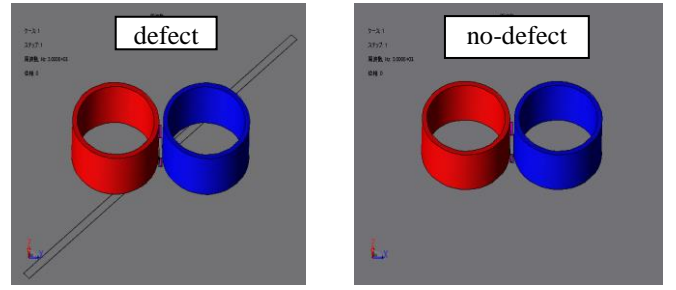


Fig1 Schematic diagram of the 3D FEM simulation

Table 1 Various constants of the tested ∞ coil

Exciting coil	
Coil outer diameter	22.4mm
Coil inner diameter	20mm
Coil length	10mm
Number of turn	75
Input voltage (peak)	3V
Frequency	2kHz
Sensing coil	
Coil outer diameter	0.9mm×2.4mm
Coil inner diameter	0.5mm×2.0mm
Coil length	6.0mm
Number of turn	100
Axis core	Mn-Zn ferrite 300

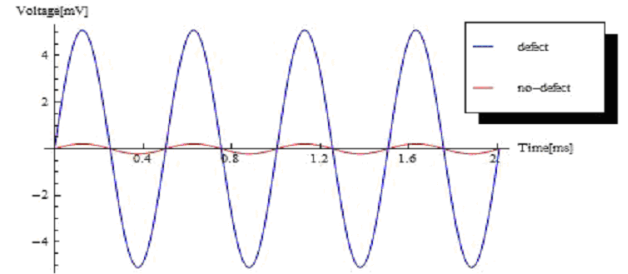

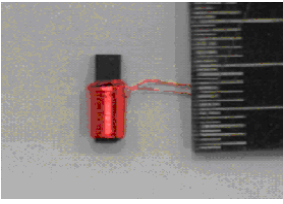
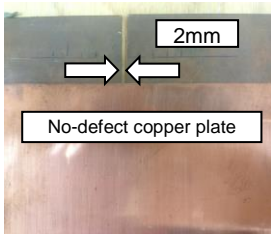


Fig 2 Induced voltage in the exciting coil

Table 2 lists the various constants of the prototype ∞ coil. Figure 3 shows the target piece and a prototype of ∞ coil. The normal target piece has been emulated by overlapping the two copper plates having 2mm width, 1mm depth. Also, the defect piece has been emulated by overlapping the one normal sheet to the other sheet having 1mm depth defect. The various constant of the prototype ∞ coil are the same used in the 3D finite element simulations.

Table 2 Various constants of the prototype ∞ coil

Exciting coil		Conductor length	4.7mm
	Diameter of conductor	0.4mm	
	Coil outer diameter	23mm	
	Coil inner diameter	20mm	
	Coil length	10mm	
	Number of turn	75	
	Number of col layers	3	
Sensing coil		Conductor length	60cm
	Diameter of conductor	0.1mm	
	Axis core	Ferrite bar (MnZn)	
	Coil outer diameter	2.4mm×2.4mm	
	Coil inner diameter	1.4mm×1.4mm	
	Coil length	6.0mm	
	Number of turn	100	
		Number of coil layers	2



(a) Target piece



(b) Prototype of the ∞ coil

Fig. 3 The target tested piece and ∞ coil

Figure 4 show the results of experiments. It looks like the results of the simulation but includes a lot of high frequency noise, where the sensor is on the backside defect and is not on any defect.

Even though the experimented signals mixed with noise in Fig.4, it is obvious that the backside defect could be detected.

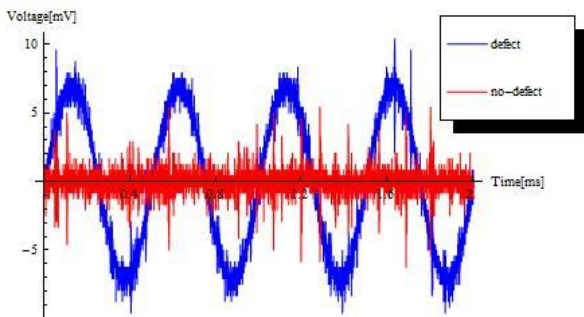


Fig 4 Induced voltage in sensing coil (experiment)

To remove the noise components from the experimentally obtained signals in Fig. 4, we employed the averaged sum method (1).

Figure 5 shows the refined signals in Fig. 4 by the averaged sum signal processing. In Fig. 5, 200 times averaged was carried out for the defect signal, and 400 times averaged was carried out for the no defect signals. Difference of the number of averaging between them is that a large signal needs not a large number of averaging because of good SN ration but a small signal requires a large number of averaging because of the bad SN ratio.

Even though the peak signal voltage of experimental results is somewhat larger that those of computed ones, the experimental signals exhibit the similar tendency to that of computed ones.

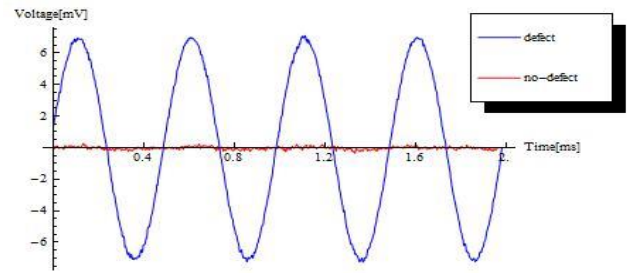


Fig 5 Induced voltage in sensing coil (averaged sum processed)

B Fourier Transform Processing

To carry out the experiment in more practical manner, the sensor coil was moved to point to point locations along a straight line as shown in Fig. 6. The sensor induced signal at each of the points was measured, where the sensor was located at the 5 points along a 20mm line.

Figure 7 shows the induced voltages at the 5 point locations. Obviously, the maximum induced voltage at the position 3 suggests the backside defect position of the target.

Figure 8 shows the signal measurement positions on the plane copper sheet. These positions are as that of the Fig. 6 to verify our approach.

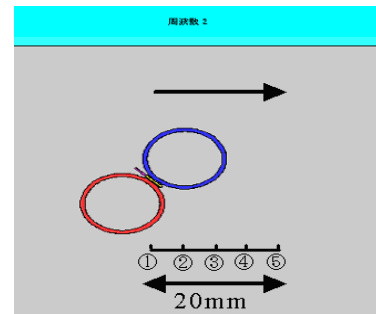


Fig 6 1D flaw detection model (simulation)

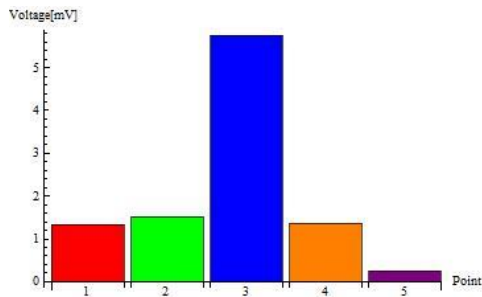


Fig 7 Sensor output voltage (simulation)

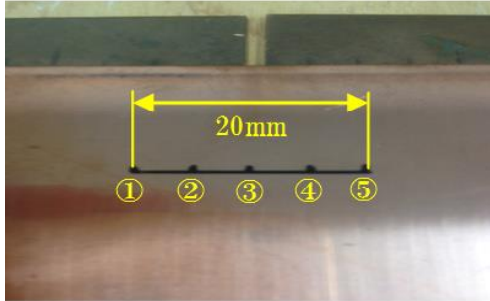


Fig 8 1D flaw detection model (experiment)

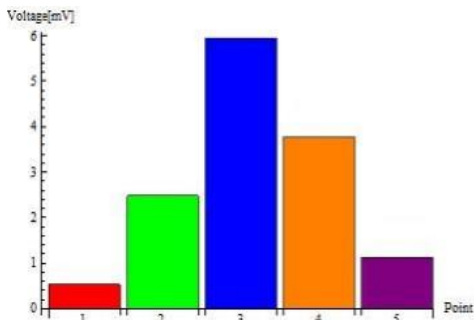


Fig 9 sensor output voltage (experiment)

The normal target piece has been emulated by overlapping the two copper plates having 2mm width, 1mm

depth. Also, the defect piece has been emulated by overlapping the one normal sheet to the other sheet having 1mm depth defect.

In any practical measurements, it is essentially measured the signals containing noise. To remove the noise signals not having the exciting current frequency, we employed the Fourier signal processing approach.

Figure 9 shows the experimentally obtained sensor output signals whose noise components were removed by the Fourier signal processing.

Comparison the results in Figs. 7 and 9 shows that their maximum values are somewhat different but their position is the same No. 3 point.

Thus, our backside defect searching by the low frequency excitation is succeeded in a first step of the project.

VIII. CONCLUSION

In the present paper, we have employed the low frequency ∞ coil excitation to search for the backside defect of the target.

As a result, it has been clarified that the low frequency ∞ coil excitation makes it possible to search for the backside defects along with the signal processing procedures enhancing the S/N ratio.

IX. REFERENCES

- [1] Hiroki Kikuchihara, Iliana Marinova, and Yoshifuru Saito, Manabu OHUCHI, Hideo MOGI and Yoshiro OIKAWA, Optimization of the Eddy Current Testing, Digest of The 15th Biennial IEEE Conference on Electromagnetic Field Computation WC4-4 pp.495, Oita Japan November 11-14 2012,
- [2] Hiroki Kikuchihara and Yoshifuru Saito, Enhance the Sensibility of the ECT Sensor, Journal of the Japan Society of Applied Electromagnetics and Mechanics, Vol.21, No.3, 2013.
- [3] Hiroki Kikuchihara, Iliana Marinova, and Yoshifuru Saito, Enhance the Sensibility of the Resonance type ECT Sensor, JAPMED'8 pp. 130-131, 2013.